ACCEPTED MANUSCRIPT
DOI of the published work: https://doi.org/10.1016/j.ijsolstr.2022.111901
International Journal of Solids and Structures, Volumes 254–255, 1 November 2022, 111901

From octagonal connection graphs belonging to the Z-Octahedron family to new tensegrity structures

Manuel Alejandro Fernández-Ruiz[a,*], Enrique Hernández-Montes[b], Luisa María Gil-Martín[c]

[a] Department of Industrial and Civil Engineering, University of Cádiz (UCA). Campus Bahía de Algeciras, Avda. Ramón Puyol, s/n. 11201 Algeciras (Cádiz), Spain. manuelalejandro.fernandez@uca.es.
*Corresponding author

[b] Department of Structural Mechanics, University of Granada (UGR). Campus Universitario de Fuentenueva s/n. 18072 Granada, Spain. emontes@ugr.es.

[c] Department of Structural Mechanics, University of Granada (UGR). Campus Universitario de Fuentenueva s/n. 18072 Granada, Spain. mlgil@ugr.es.

Abstract

A tensegrity family is a group of tensegrity structures that share a common connectivity pattern. The Octahedron, the Z-Octahedron, and the X-Octahedron families are examples of these groups found in the literature. In this work, a new graphical representation of the members of the Z-Octahedron family based on octagonal cells is presented. These new elementary cells are composed of eight nodes and two struts. In addition, a new member of the family is introduced: the Z-triple-expanded octahedron. New tensegrity structures from the Z-Octahedron family are obtained by modifying the connectivity pattern of the elements that make up the octagonal cell. Several element groupings have been considered in order to find different equilibrium configurations. The values of the force density or force:length ratio that lead to stable and super-stable tensegrity forms have been computed analytically. It has been proved that the Z-Octahedron family is a good source of new tensegrity forms.

Keywords: Tensegrity; Z-Octahedron family; Octagonal cell; Analytical form-finding; Force density method.

1. Introduction

Tensegrity structures are pin-jointed, free-standing, and pre-stressed, and they are

composed of compression (struts) and tension (cables) members that are self-equilibrated. The unique mechanical and mathematical properties of these structures mean that they have applications in many fields, such as robotics (Graells Rovira and Mirats Tur, 2009; Lee et al., 2020; Liu et al., 2022), biology (Fraldi et al., 2021; Suma et al., 2020), mechanical engineering (Boni and Royer-Carfagni, 2021; Kan et al., 2019), civil engineering (Bel Hadj Ali et al., 2010; Veuve et al., 2016), and aerospace engineering (Chen et al., 2020; Tibert and Pellegrino, 2002). Tensegrity structures can also be used as dissipative devices for earthquake-proof structures (Fraternali and Santos, 2019; Singh et al., 2020). In addition, tensegrity metamaterials can be used in impact protection and energy dissipation systems (Bauer et al., 2021; Ma et al., 2018).

A tensegrity should fulfill the following conditions (Zhang and Ohsaki, 2015): *i)* the tensegrity is free-standing without any support; *ii*) it is composed of only two types of members (cables in tension and struts in compression); *iii*) the struts are not in contact with each other at their ends, and *iv*) the self-weight of the tensegrity is negligibly small in comparison with the member forces. The tensegrity structures shown in this work fulfill all the conditions listed above. In practice, in addition to the preceding conditions, tensegrity structures should satisfy some other requirements. Some examples of these requirements are: members should not intersect with each other, and both the buckling of the struts and the yielding of the cables must be prevented. There are some optimization methods that consider member intersection (Xu et al., 2016) and buckling constraints (Xu et al., 2018) in order to avoid these situations. The member intersection and the potential local buckling of compression members have not been considered in the present work.

The creation of these types of interesting structures is complex because tensegrities do not exhibit very intuitive principles (Gómez-Jáuregui, 2010). In addition, novel applications such as biomechanical structural models and mechanical metamaterials require large-scale tensegrity structures, which increase the complexity of the design procedure. One of the main sources of tensegrity structures are regular polyhedrons, including simple polyhedral tensegrities, prismatic tensegrities, and truncated polyhedral tensegrities (Yin et al., 2020; Zhang et al., 2019, 2021, 2013). However, truncated polyhedral tensegrities are limited by the five types of convex regular polyhedrons: tetrahedron, cube, octahedron, dodecahedron, and icosahedron.

Another way to construct a tensegrity structure is by assembling elementary modules together in a specific manner. In Murakami et al. (Murakami and Nishimura, 2001), the

static and dynamic characterization of truncated regular polyhedral modules is studied. Rhode-Barbarigos et al. (Rhode-Barbarigos et al., 2010) and Feron et al. (Feron et al., 2019) proposed the use of tensegrity modules as elementary building modules in the design of pedestrian bridges. In line with this design procedure, Li et al. (Li et al., 2010) show that tensegrity structures can be constructed by assembling one-bar elementary cells. Pugh (Pugh, 1976) defines two main classes of tensegrity structures, named "rhombic" (or "diamond") and "zig-zag" systems. Most rhombic and zig-zag tensegrities can be considered as assemblages of rhombic and Z-shaped cells, respectively (see Figure 1).

Figure 1. Rhombic (a) and Z-shaped (b) elementary cells. Thick gray lines and thin black lines correspond to struts and cables, respectively. Adapted from (Fernández-Ruiz et al., 2020).

Finally, tensegrity families are another great source of tensegrity structures. A tensegrity family is a group of tensegrity structures that share a common connectivity pattern (Fernández-Ruiz et al., 2022, 2021, 2020, 2019). The Octahedron (Fernández-Ruiz et al., 2022, 2019), the Z-Octahedron (Fernández-Ruiz et al., 2020), and the X-Octahedron (Fernández-Ruiz et al., 2021) families are examples of families of tensegrity structures found in the literature. The greatest advantage of the design of tensegrity structures based on tensegrity families is that they can be used to construct new tensegrity forms based on topology instead of using geometrical intuition. Each member of the family has all the previous members of the family as folded forms (Fernández-Ruiz et al., 2019). Folded forms are tensegrity structures where some nodes in the equilibrium configuration share the same position in the space (Hernández-Montes et al., 2018), while full forms are tensegrity structures where all the nodes have different positions in the equilibrium shape (Hernández-Montes et al., 2018). With this property in mind, a full form can be considered as the folded form of the subsequent member of the family, obtaining new tensegrities with a higher number of nodes, struts, and cables.

In this work, a new member of the Z-Octahedron family is presented: the Z-triple-expanded octahedron (which is composed of 48 nodes, 24 struts, and 72 cables). In addition, a new graphical representation of the members of the Z-Octahedron family based on octagonal cells is proposed. New tensegrity structures are constructed by

changing the connectivity pattern of the members of the elementary octagonal cell of the Z-Octahedron family. Several element groupings have been considered in order to find different equilibrium configurations. An analytical form-finding method (Fernández-Ruiz et al., 2019; Hernández-Montes et al., 2018) based on the Force Density Method (FDM) (Linkwitz and Schek, 1971; Schek, 1974) is used to solve the self-equilibrated states of the tensegrities shown in this work. Finally, it has been proved that the introduction of additional cables in the octagonal cells can result in an improvement of the stability of a tensegrity.

The tensegrity structures presented in this work could have promising engineering applications. New research in different fields could be derived from the application of these new tensegrities. Among others examples, they could be considered as a unit of tensegrity mass-spring chains (Amendola et al., 2018; Fraternali et al., 2014).

2. A new graphical representation of the Z-Octahedron family

2.1 The Z-Octahedron family

The Z-Octahedron family has already been presented in Fernández-Ruiz et al. (Fernández-Ruiz et al., 2020). The first two members, the Z-expanded octahedron and the Z-double-expanded octahedron are defined by using Z-shaped elementary cells (see Figure 2.a and Figure 2.b, respectively).

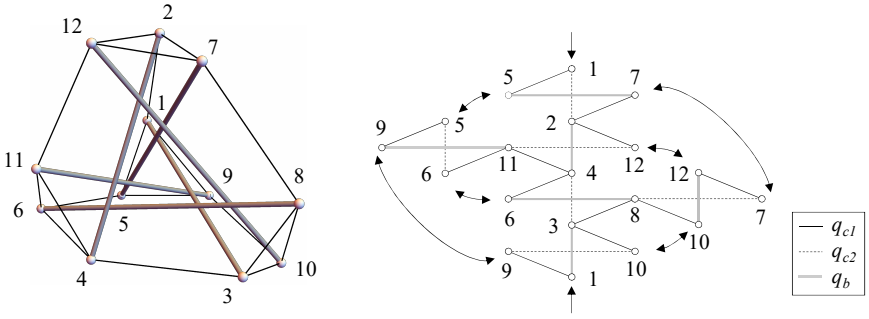

(a)

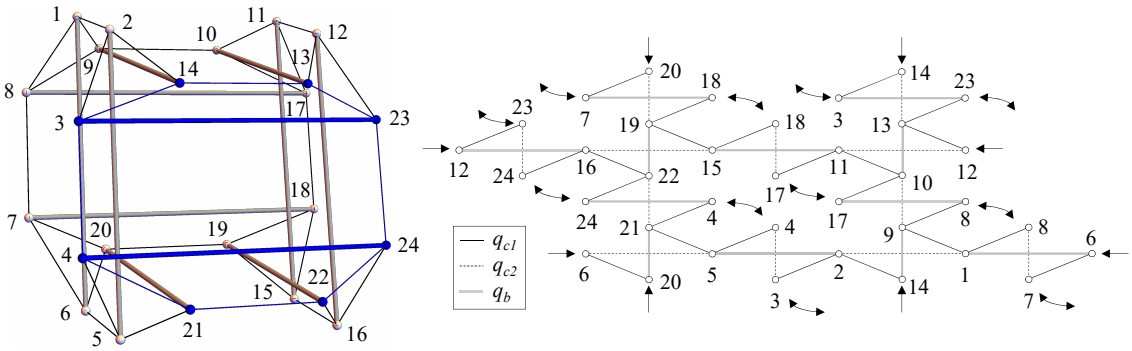

(b)

Figure 2. A Z-expanded octahedron (a) and a Z-double-expanded-octahedron (b) together with their corresponding plane connection graphs. Gray lines, black lines, and dashed black lines correspond to struts, type 1 cables, and type-2 cables, respectively. The plane connection graphs have been adapted from (Fernández-Ruiz et al., 2020).

The analytical form-finding method based on FDM that is employed in this work for the design of tensegrity structures is summarized in Appendix A, as well as the stability and super-stability criterions.

In Fernández-Ruiz et al. (Fernández-Ruiz et al., 2020), two types of cables are identified (type 1 and type 2) in the two tensegrities of the Z-Octahedron family shown in Figure 2. Consequently, two positive values of the force:length ratio are considered for cables (q_{c1} and q_{c2} for type 1 and type 2 cables, respectively). On the other hand, only one value of force:length ratio is considered for struts (q_b, negative). The force:length ratio, q, is defined as the ratio between the axial force and the length of each member of the tensegrity. Furthermore, two independent normalized force:length ratios taken as $Q_1 = -q_{c1}/q_b$ and $Q_2 = -q_{c2}/q_b$ are considered. Note that, by definition, Q_1 and Q_2 are positive.

The Z-expanded octahedron (see Figure 2.a) is composed of 6 Z-shaped cells (12 nodes, 6 struts, and 18 cables). The solutions given by the analytical form-finding method considering $q_{c1} = q_{c2}$ (and consequently, $Q_1 = Q_2$) have already been presented in (Fernández-Ruiz et al., 2020): $Q_1 = 1/10\left(11-\sqrt{41}\right)$ and $Q_1 = 1/10\left(11+\sqrt{41}\right)$. Other solutions are obtained, but they are ruled out because Q_1 has negative values or it is equal to zero. The solution, $Q_1 = 1/10\left(11+\sqrt{41}\right)$, leads to a super-stable equilibrium configuration (the Z-expanded octahedron, see Figure 2.a), while $Q_1 = 1/10\left(11-\sqrt{41}\right)$ leads to a tensegrity which cannot not be considered as being either super-stable (it does not fulfill condition (*ii*) of the super-stability criterion) or stable (taking into consideration the material properties shown in Appendix A).

The next member of the Z-Octahedron family, the Z-double-expanded octahedron (see Figure 2.b) composed of 12 Z-shaped cells (24 nodes, 12 struts, and 36 cables), has already been presented in (Fernández-Ruiz et al., 2020). The solutions of the form-finding problem in this case assume that $q_{c1} = q_{c2}$ are $Q_1 = 1/10\left(11-\sqrt{41}\right)$, $Q_1 = 1/10\left(11+\sqrt{41}\right)$ and $Q_1 = 7/3$. The solution corresponding to $Q_1 = 7/3$ leads to the super-stable full form of the Z-double-expanded octahedron (see Figure 2.b),

$Q_1 = 1/10\left(11+\sqrt{41}\right)$, which corresponds to the unstable folded form of the Z- double-expanded octahedron, while $Q_1 = 1/10\left(11-\sqrt{41}\right)$ leads to an unstable tensegrity structure.

In Fernández-Ruiz et al. (Fernández-Ruiz et al., 2020), a higher number of different values of force:length ratio is studied.

2.2 Octagonal connection graphs

A plane connection graph is a graphical representation of the connectivity between the nodes of a tensegrity (Fernández-Ruiz et al., 2019). The plane connection graph has a key role in the design of tensegrity structures because it is the basis for the construction of connectivity matrix **C** (defined in Appendix A) of the tensegrity. Figure 2 shows the plane connection graphs based on Z-shaped elementary cells of both the Z-expanded octahedron and the Z-double expanded octahedron (Fernández-Ruiz et al., 2020). These plane connection graphs are obtained by replacing the rhombic cells of the tensegrities of the Octahedron family defined in (Fernández-Ruiz et al., 2019) by Z-shaped cells.

In this piece of work, an alternative plane connection graph is presented that is based on a new type of cell: the octagonal cell. In Figure 2.b, two struts and eight cables of the Z-double-expanded octahedron have been highlighted in blue (for the interpretation of the references to color, the reader is referred to the online version of this article). These struts and cables can be considered as making up an octagonal cell. Accordingly, the Z-double expanded octahedron can be constructed by assembling six octagonal cells (see Figure 3). This new plane connection graph (called an octagonal connection graph) is equivalent to the one shown in Figure 2.b.

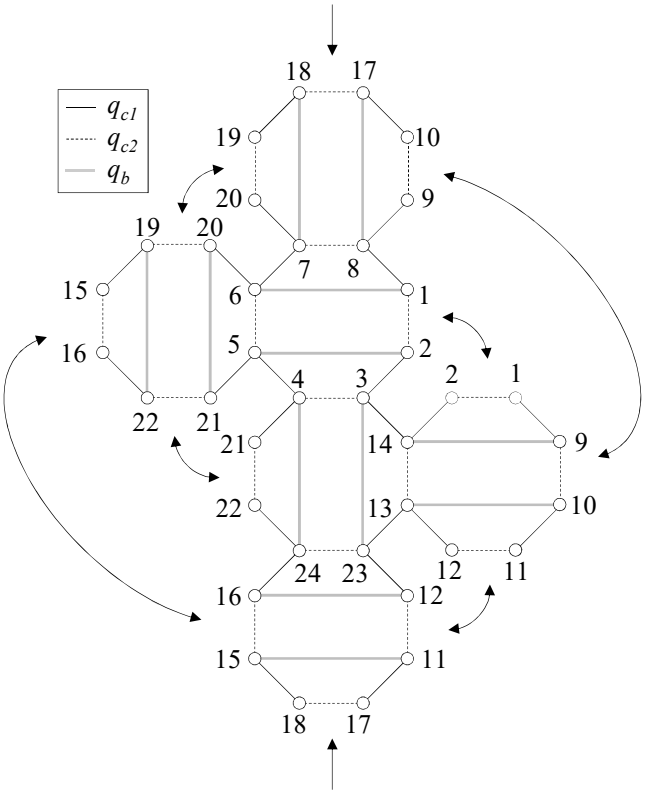

Figure 3. New octagonal connection graph of the Z-double expanded octahedron. Gray lines, black lines, and dashed black lines correspond to struts, type 1 cables, and type-2 cables, respectively.

It should be highlighted that each of the elementary cells shown in Li et al. (Li et al., 2010) and those used in the Octahedron (Fernández-Ruiz et al., 2022, 2019), the Z-Octahedron (Fernández-Ruiz et al., 2020), and the X-Octahedron (Fernández-Ruiz et al., 2021) tensegrity families only have one strut each. On the other hand, the new octagonal cell has two struts and eight cables. This new type of cell opens up a new range of possibilities for defining new tensegrity structures.

3. The Z-triple-expanded octahedron

It is interesting to note that the connectivity between the cells of the octagonal connection graph of the Z-double expanded octahedron (see Figure 3) follows the same pattern as that of the Z-expanded octahedron that is based on Z-shaped elementary cells (see Figure 2.a). Therefore, the octagonal connection graph of the Z-triple expanded octahedron (see Figure 4) has been constructed following the same connection pattern as that of the Z-double-expanded octahedron when Z-shaped cells are considered (see Figure 2.b).

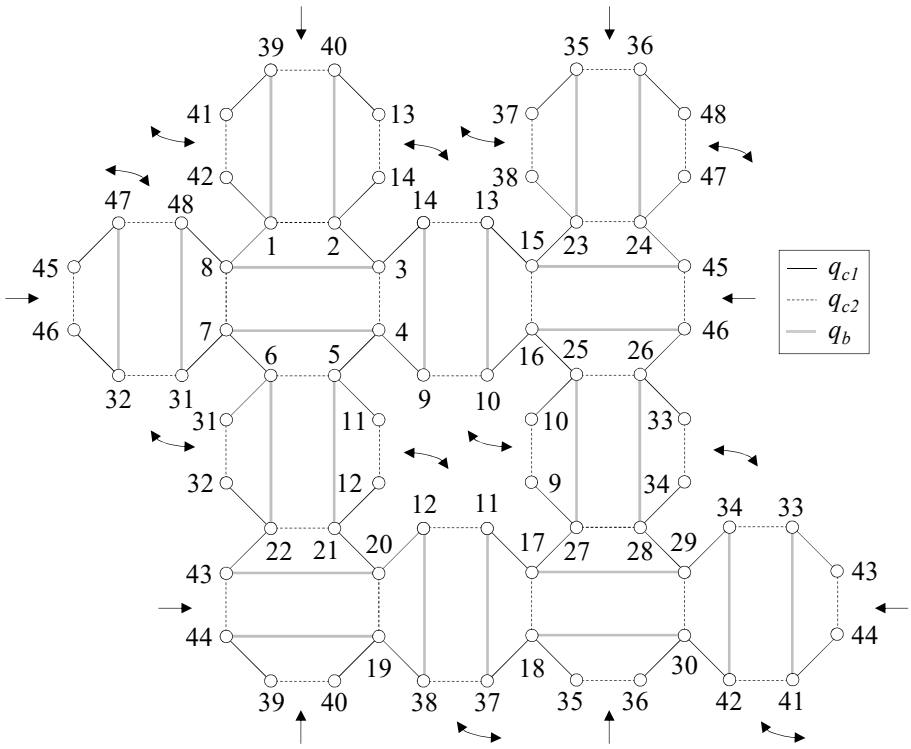

Figure 4. Octagonal connection graph of the Z-triple-expanded octahedron. Gray lines, black lines, and dashed black lines correspond to struts, type 1 cables, and type-2 cables, respectively.

Figure 4 shows that the Z-triple-expanded octahedron is composed of 12 octagonal cells (48 nodes, 24 struts, and 72 cables). For this tensegrity, the solutions of the form-finding problem are $Q_1 = 1/10\left(11-\sqrt{41}\right)$, $Q_1 = 1/10\left(11+\sqrt{41}\right)$, $Q_I = 7/3$, $Q_I = 2/5$, $Q_1 = 1/7\left(10-\sqrt{30}\right)$ and $Q_1 = 1/7\left(10+\sqrt{30}\right)$. The solutions $Q_1 = 1/10\left(11+\sqrt{41}\right)$ and $Q_I = 7/3$ correspond to the Z-expanded octahedron and the Z-double-expanded octahedron, whose members are duplicated and quadruplicated, (the first one is unstable and the second one is super-stable), respectively. Therefore, it can be concluded that the Z-triple-expanded octahedron resulting from the octagonal connection graph shown in Figure 4 belongs to the Z-Octahedron family. It has been verified that the solutions $Q_1 = 1/10\left(11-\sqrt{41}\right)$, $Q_I = 2/5$ and $Q_1 = 1/7\left(10-\sqrt{30}\right)$ correspond to unstable tensegrity structures. The solution $Q_1 = 1/7\left(10+\sqrt{30}\right)$ leads to the full-form of the Z-triple-expanded octahedron (see Figure 5), which is not super-stable because its corresponding force density matrix, **D**, is not positive semi-definite (in this case some eigenvalues are very close to 0, but they are negative). However, and according to the material properties shown in Appendix A, the Z-triple-expanded octahedron is a stable

tensegrity.

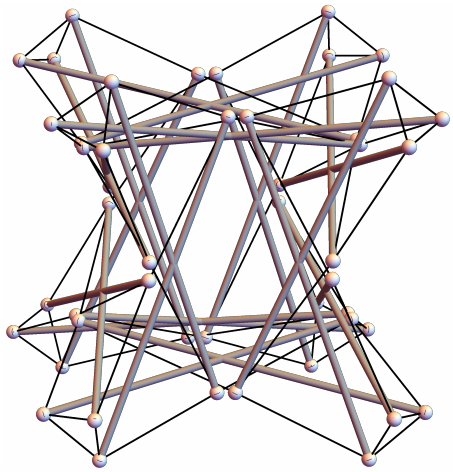

Figure 5. Z-triple-expanded octahedron with $Q_1 = 1/7\ (10+\sqrt{30})$ and $q_b = -1$

4. New tensegrity structures based on the Z-Octahedron family

New tensegrity structures can be defined by replacing the connectivity pattern of the elementary octagonal cells of the plane connection graphs of the Z-Octahedron family. Let us consider, in addition to the previously considered octagonal cell (see Figures 3 and 4 and the type 1 octagonal cell in Figure 6.a), another two types of octagonal cells (see types 2 and 3 in Figure 6). Figure 6 shows that the struts are crossed in a type 2 octagonal cell, and two additional crossed cables connecting opposite nodes of the cell are included in a type 3 cell.

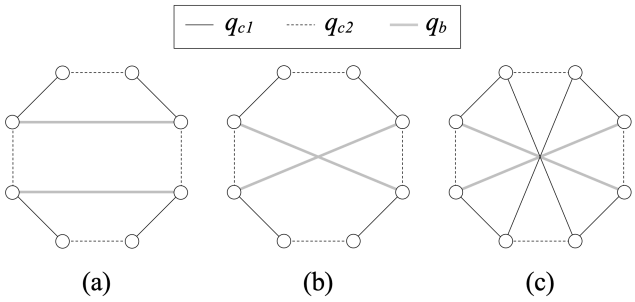

Figure 6. Octagonal cell type 1 (a), type 2 (b), and type 3 (c). Gray lines, black lines, and dashed black lines correspond to struts, type 1 cables, and type-2 cables, respectively.

4.1 Type 2 octagonal cell

4.1.1 Type-2-double-expanded octahedron

The plane connection graph of the type-2-double-expanded octahedron is obtained by replacing the type 1 octagonal cells from Figure 3 with type 2 octagonal cells (Figure

6.b).

If only two values of q are considered ($q_{c1} = q_{c2}$, and so $Q_1 = Q_2$), the solutions of the form-finding problem that lead to a full form of the tensegrity are: $Q_1 = 1/3\left(5-\sqrt{13}\right)$ and $Q_1 = 1/3\left(5+\sqrt{13}\right)$. The solution $Q_1 = 1/3\left(5-\sqrt{13}\right)$ leads to an unstable tensegrity but, for $Q_1 = 1/3\left(5+\sqrt{13}\right)$, a super-stable tensegrity is obtained: the type-2-double-expanded octahedron (see Figure 7).

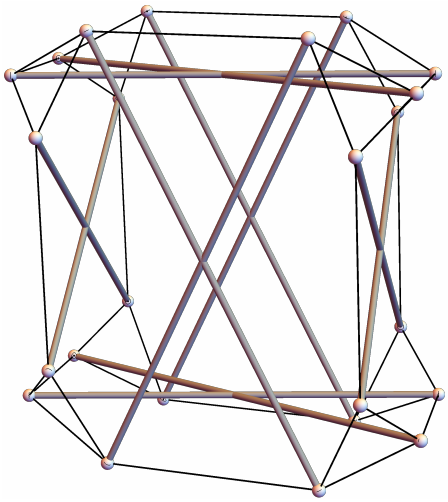

Figure 7. Type-2-double-expanded octahedron with $Q_1 = Q_2 = 1/3\ (5+\sqrt{13})$ and $q_b = -1$

If three values of q are considered instead of two, as indicated in Figure 6.b (q_{c1}, q_{c2} and q_b), then the solution of the form-finding problem is the one shown in Eq. (1). It should be highlighted that other solutions can also be obtained, but they have been ruled out because they lead to folded forms, or because Q_1 and/or Q_2 have negative values (and by definition, both must be positive).

$$Q_2 = \frac{2\left(-2+3Q_1\right)}{-4+3Q_1} \tag{1}$$

Figure 8.a shows the curve, $Q_1 - Q_2$, which corresponds to Eq. (1). It is important to note that not all the $Q_1 - Q_2$ pairs resulting from Eq. (1) lead to super-stable or stable tensegrities. Hence, the next step is to study whether the super-stability conditions numbered in Appendix A are fulfilled or not. First of all, the conditions $Q_1 > 0$ and $Q_2 > 0$ are checked. In the regions $0 < Q_1 < 2/3$ and $Q_1 > 4/3$, both Q_1 and Q_2 are positive. Secondly, condition (i) of the super-stability criterion is imposed on the structure, for which the rank deficiency of the resulting matrix **D** must be exactly $d + 1$ ($d = 3$ in three-dimensional tensegrities, see Appendix A). It has been verified that all the

tensegrity structures in the regions $0 < Q_1 < 2/3$ and $Q_1 > 4/3$ have exactly 4 zero eigenvalues. Condition (ii) of the super-stability criterion indicates that matrix **D** must be positive semi-definite. This condition is fulfilled in region $Q_1 > 4/3$. Figure 8.b shows the minimum eigenvalue of matrix **D** for all the $Q_1 - Q_2$ pairs obtained from Eq. (1) in region $0 < Q_1 < 2/3$, considering $q_b = -1$. It can be seen that there is always a negative eigenvalue and so tensegrity forms resulting from Eq. (1) in region $0 < Q_1 < 2/3$ do not fulfill condition (ii) of super-stability. Finally, and according to condition (iii) of the super-stability criterion, the rank of the geometry matrix, **G**, must be $(d^2+d)/2 = 6$. The tensegrity forms obtained from Eq. (1) in region $Q_1 > 4/3$ have a geometry matrix with a rank of six. Consequently, the tensegrities of region $Q_1 > 4/3$ can be considered as super-stable. On the contrary, tensegrity forms obtained from Eq. (1) in region $0 < Q_1 < 2/3$ are unstable. The study of the super-stability is summarized in Table 1.

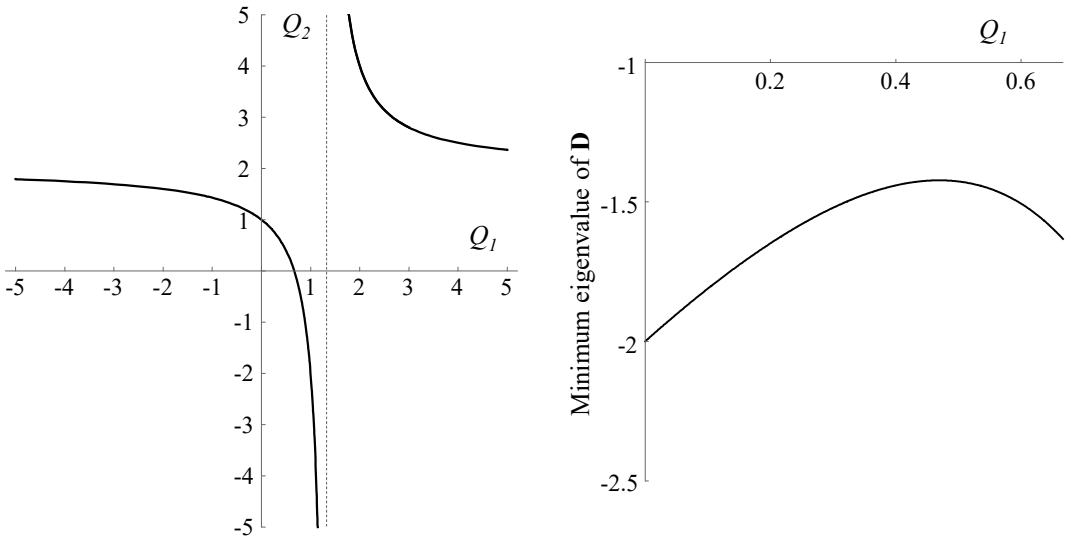

(a) (b)

Figure 8. $Q_1 - Q_2$ self-equilibrium curves of the type-2-double-expanded octahedron (Eq. (1)) (a) and minimum eigenvalue of D for the Q_1 - Q_2 graph of Eq. (1) in the region $0 < Q_1 < 2/3$, considering $q_b = -1$.

Table 1. Super-stability analysis of the type-2-double-expanded octahedron considering three values of *q*. Condition (i): force density matrix D has exactly four zero-eigenvalues. Condition (ii): matrix D is positive semi-definite. Condition (iii): geometry matrix G has a rank of 6.

Solution	Q_1 and $Q_2 > 0$	Condition (i)	Condition (ii)	Condition (iii)
Eq. (1)	$0 < Q_1 < 2/3$	✓	×	-

	$Q_1 > 4/3$	✓	✓	✓

Figure 9 shows three super-stable equilibrium configurations of the type-2-double-expanded octahedron for different $Q_1 - Q_2$ pairs of Eq. (1) in region $Q_1 > 4/3$. As Q_1 increases in Eq. (1), the resultant tensegrity resembles more a truncated cube (see Figure 9).

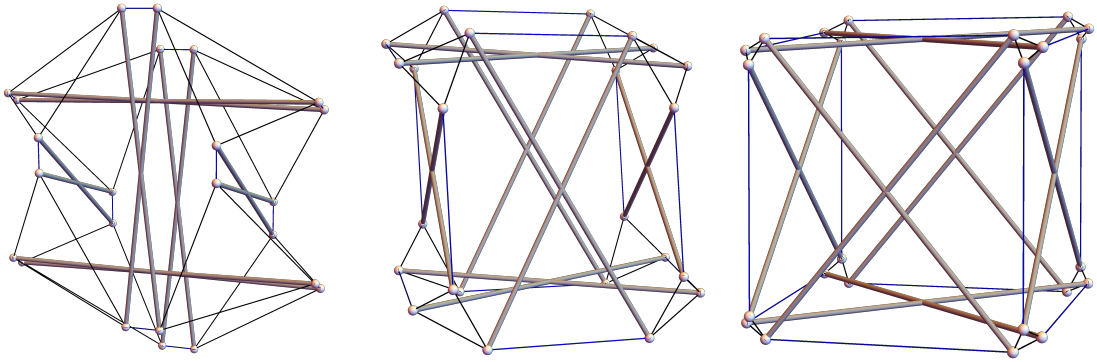

(a) (b) (c)

Figure 9. Equilibrium shapes of the type-2-double-expanded octahedron considering different values of q. Q_1 = 1.5 & Q_2 = 10 (Eq. (1)) & q_b = -1 (a); Q_1 = 3 & Q_2 = 2.8 (Eq. (1)) & q_b = -1 (b); Q_1 = 8 & Q_2 = 2.2 (Eq. (1)) & q_b = -1 (c). Black and blue cables correspond to q_{c1} and q_{c2}, respectively and gray bars to q_b.

4.1.2 Type-2-triple-expanded octahedron

As previously mentioned, the plane connection graph of the type-2-triple-expanded octahedron is constructed by replacing the type 1 octagonal cells from Figure 4 with type 2 octagonal cells. It should be highlighted that the connectivity pattern between the type 2 octagonal cells in the type-2-triple-expanded octahedron is the same as the one that corresponds to the Z-triple-expanded octahedron (see Figure 4). If only two values of q are considered ($Q_1 = Q_2$), the solutions of the form-finding problem that leads to a full-form are $Q_1 = 3/70\left(31 - 3\sqrt{29}\right)$ and $Q_1 = 3/70\left(31 + 3\sqrt{29}\right)$. Both solutions lead to unstable tensegrity forms. Other solutions are also obtained, including $Q_1 = 1/3\left(5 + \sqrt{13}\right)$, which corresponds to the type-2-double-expanded octahedron, whose nodes and members are duplicated (folded form). Given the complexity of the system of equations obtained, a higher number of different values of q are not considered due to the high computational cost. limitations in the calculation capacity.

4.2 Octagonal cell type 3

4.2.1 Type-3-double-expanded octahedron

As in the previous case, the plane connection graph of the type-3-double-expanded octahedron is obtained by replacing the type 1 octagonal cells of Figure 3 with type 3 octagonal cells (Figure 6.c). The type 3 double-expanded octahedron is composed of 6 type-3 octagonal cells (24 nodes, 12 struts, and 48 cables). The solutions of the form-finding problem that consider $q_{c1} = q_{c2}$ (and consequently $Q_1 = Q_2$) that lead to a full form are $Q_1 = 1/17\left(15-\sqrt{89}\right)$ and $Q_1 = 1/17\left(15+\sqrt{89}\right)$. Solution $Q_1 = 1/17\left(15-\sqrt{89}\right)$ leads to an unstable tensegrity, but $Q_1 = 1/17\left(15+\sqrt{89}\right)$ corresponds to a super-stable tensegrity called type-3-double-expanded octahedron (see Figure 10).

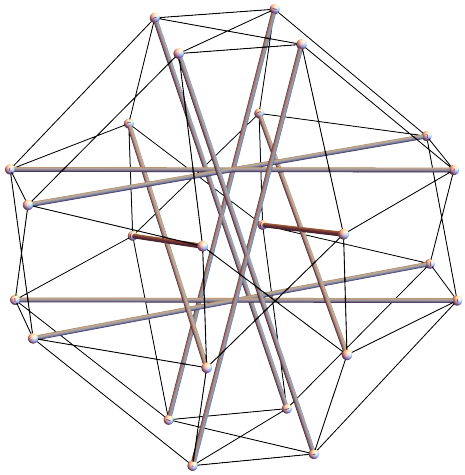

Figure 10. Type-3-double-expanded octahedron with $Q_1 = Q_2 = 1/17\ (15+\sqrt{89})$ and $q_b = -1$

If three values of q are considered, as indicated in Figure 6.c (q_{c1}, q_{c2} and q_b), the only solution that leads to full forms is shown in Eq. (2).

$$Q_2 = \frac{2\left(4-11Q_1+5Q_1^2\right)}{8-7Q_1} \tag{2}$$

Figure 11.a shows the $Q_1 - Q_2$ representation that corresponds to Eq. (2). As in Section 4.1.1, a study of the super-stability is carried out depending on the value of the $Q_1 - Q_2$ pairs (this study is summarized in Table 2). Tensegrity structures for which $8/7 < Q_1 < 1/10\left(11+\sqrt{41}\right)$ can be considered as super-stable while if $0 < Q_1 < 1/10\left(11-\sqrt{41}\right)$, then the tensegrities are unstable.

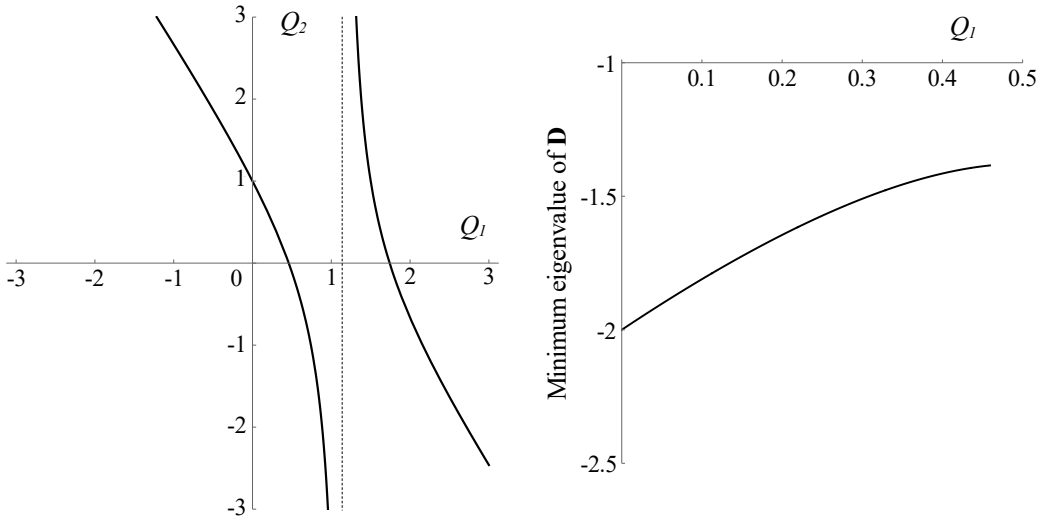

Figure 11. $Q_1 - Q_2$ self-equilibrium curves of the type-3-double-expanded octahedron (Eq. (2)) (a) and the minimum eigenvalue of D for the Q_1 - Q_2 graph of Eq. (2) in region $0 < Q_1 < 1/10\ (11-\sqrt{41})$ considering $q_b = -1$.

Table 2. Super-stability analysis of the type-3-double-expanded octahedron considering three values of q. Condition (i): force density matrix D has exactly four zero-eigenvalues. Condition (ii): matrix D is positive semi-definite. Condition (iii): geometry matrix G has a rank of 6.

Solution	Q_1 and $Q_2 > 0$	Condition (i)	Condition (ii)	Condition (iii)
Eq. (2)	$0 < Q_1 < 1/10\ (11-\sqrt{41})$	✓	×	-
	$8/7 < Q_1 < 1/10\ (11+\sqrt{41})$	✓	✓	✓

Figure 12 shows three super-stable equilibrium configurations of the type-3-double-expanded octahedron considering several $Q_1 - Q_2$ pairs of Eq. (2) in region $8/7 < Q_1 < 1/10\left(11+\sqrt{41}\right)$.

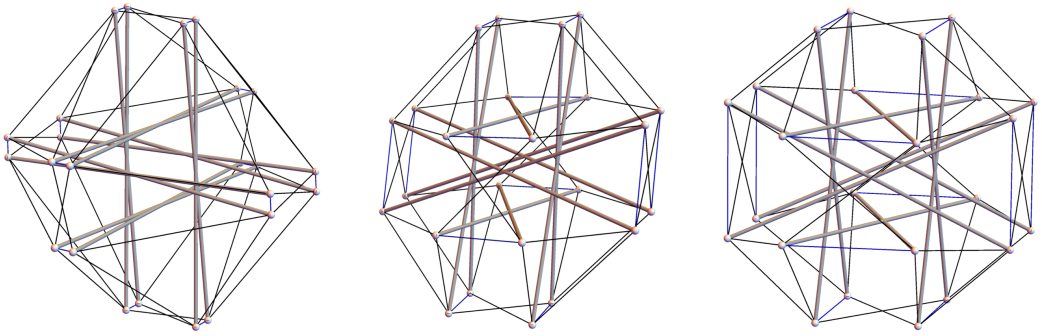

Figure 12. Equilibrium shapes of the type-3-double-expanded octahedron considering different values of q. $Q_1 = 1.2$ & $Q_2 = 10$ (Eq. (2)) & $q_b = -1$ (a); $Q_1 = 1.5$ & $Q_2 = 1$ (Eq. (2)) & $q_b = -1$ (b); $Q_1 =$

1.7 & Q_2 = 0.13 (Eq. (2)) & q_b = -1 (c). Black and blue cables correspond to q_{c1} and q_{c2}, respectively and gray bars to q_b.

4.2.2 Type-3-triple-expanded octahedron

The plane connection graph of the type-3-triple-expanded octahedron is constructed by replacing the type 1 octagonal cells from Figure 4 with type 3 octagonal cells. The connectivity pattern between the type 3 octagonal cells in the type-3-triple-expanded octahedron is the same than the one corresponding to the Z-triple-expanded octahedron (see Figure 4) and to the type-2-triple-expanded octahedron. The type-3-triple-expanded octahedron is composed of 12 type 3 octagonal cells (48 nodes, 24 struts, and 96 cables). As in Section 4.1.2, only two values of q are considered ($q_{c1} = q_{c2}$, and so $Q_1 = Q_2$) due to the high computational cost. The solutions of the form-finding problem that lead to a full-form are $Q_1 = 1/346\left(379+3\sqrt{3581}\right)$ and $Q_1 = 1/346\left(379-3\sqrt{3581}\right)$. The solution $Q_1 = 1/346\left(379-3\sqrt{3581}\right)$ leads to an unstable tensegrity, but the solution $Q_1 = 1/346\left(379+3\sqrt{3581}\right)$ corresponds to a super-stable tensegrity called type-3-triple-expanded octahedron (see Figure 13). Other solutions are also obtained, including $Q_1 = 1/17\left(15+\sqrt{89}\right)$, which corresponds to the type-3-double-expanded octahedron, whose nodes and members are duplicated (folded form).

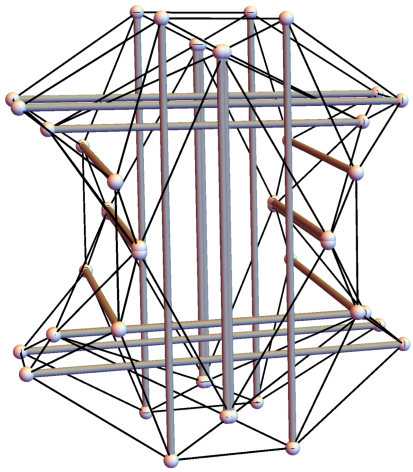

Figure 13. Type-3-triple-expanded octahedron with $Q_1 = Q_2$ = 1/346 (379+3√3581) and q_b = -1

It is interesting to note that the introduction of additional cables means an improvement in the stability of the tensegrity because the type-2-triple-expanded octahedron is unstable, while the type-3-triple-expanded octahedron is a super-stable tensegrity. Hence, the type of octagonal elementary cell used to construct the connectivity pattern

has a significant amount of influence on the tensegrity obtained, especially related to number of cables or tensioned members. The introduction of these two cables per octagonal cell is responsible for the difference in the stability of type 2 and type 3 triple-expanded octahedron tensegrity structures.

4.3. Octagonal connection graphs for the expanded octahedron

Special attention is paid to the Z-expanded octahedron (Figure 2.a) when an octagonal elementary cell is used. Figure 14 shows the octagonal connection graph of the Z-expanded octahedron (which is equivalent to the one shown in Figure 2.a). The comparison of this figure with Figure 3 and Figure 4 shows that, in Figure 14, some of the external nodes are permuted, and so the connection pattern is slightly different.

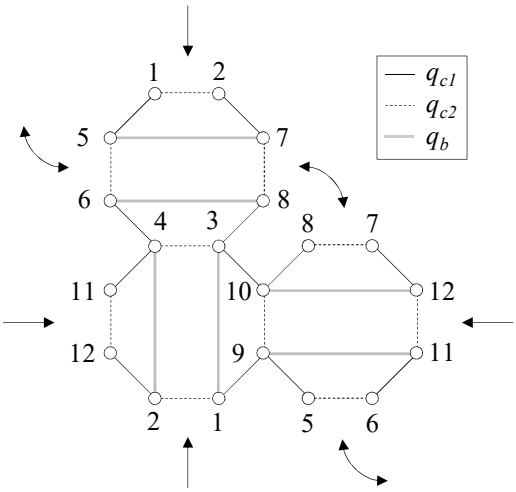

Figure 14. Octagonal connection graph of the Z-expanded octahedron. Gray lines, black lines, and dashed black lines correspond to struts, type 1 cables, and type-2 cables, respectively.

As in the previous sections, the type-1 octagonal cells in Figure 14 have been replaced by type 2 and type 3 octagonal cells (see Figure 6), and just one or two values of the force:length ratios for cables have been considered. The results obtained that correspond to super-stable tensegrities are summarized in Table 3.

Table 3. Z-expanded octahedron. Summary of super-stable configurations

Octagonal cell	$Q_1 = Q_2 = -q_{c1}/q_b$	$Q_1 = -q_{c1}/q_b$ & $Q_2 = -q_{c2}/q_b$	
	Solution	Solution	Region
Type 1	$Q_1 = 1/10\left(11+\sqrt{41}\right)$	$Q_2 = \frac{-2+6Q_1-3Q_1^2+\sqrt{4-8Q_1+8Q_1^2-12Q_1^3+9Q_1^4}}{4\left(-1+Q_1\right)}$	$Q_1 > 1$
Type 2			
Type 3	$Q_1 = 3/4$	$Q_2 = \frac{-2+10Q_1-11Q_1^2+\sqrt{4-8Q_1-8Q_1^2-4Q_1^3+41Q_1^4}}{4\left(-1+2Q_1\right)}$	$1/2 < Q_1 < 1/10\left(11+\sqrt{41}\right)$

Table 3 shows that the solution of the form-finding problem of type 1 and type 2 expanded octahedrons is exactly the same. In addition, this solution has been studied in Fernández-Ruiz et al. (Fernández-Ruiz et al., 2020). On the other hand, Figure 15 shows several equilibrium configurations of the type-3-expanded octahedron that consider different $Q_1 - Q_2$ pairs.

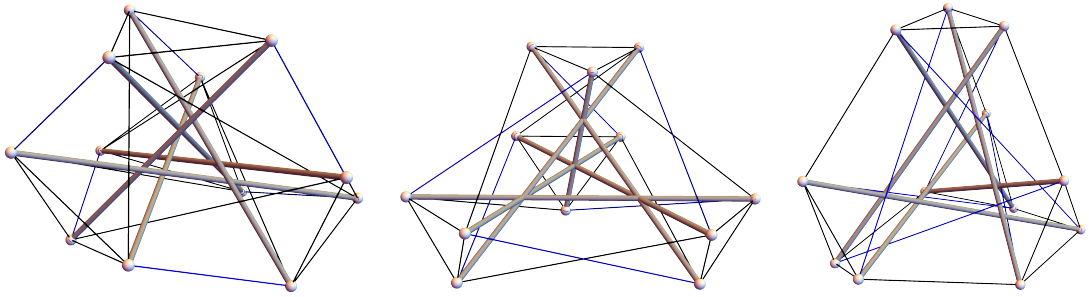

(a) (b) (c)

Figure 15. Equilibrium shapes of the type-3- expanded octahedron considering different values of q according to Table 3. $Q_1 = 0.60$ & $Q_2 = 1.15$ & $q_b = -1$ (a); $Q_1 = Q_2 = 3/4$ & $q_b = -1$ (b); $Q_1 = 1.60$ & $Q_2 = 0.09$ & $q_b = -1$ (c). Black and blue cables correspond to q_{c1} and q_{c2}, respectively and gray bars to q_b.

4.4. Summary

All the values of the force:length ratios obtained in this work which lead to stable or super-stable full-forms of tensegrities are summarized in Figure 16.

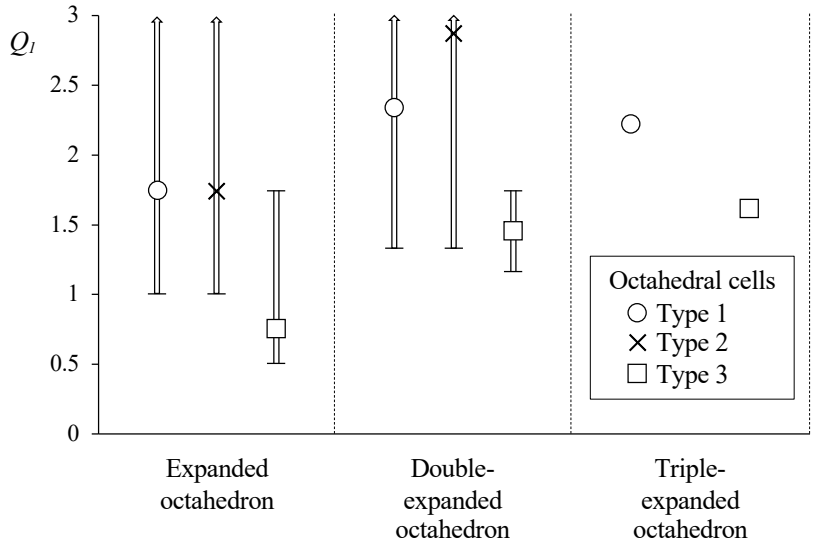

Figure 16. Range of values of Q_1 for which stable and super-stable tensegrities are obtained for all the types of octagonal cells studied in the work (see Figure 6). Circles, crosses, and squares indicate the $Q_1 - Q_2$ pair for which $Q_1 = Q_2$ in the case of type 1, type 2, and type 3 octagonal cells respectively.

5. Conclusions

The Z-expanded octahedron and the Z-double-expanded octahedron are constructed by assembling Z-shaped cells. In this piece of work, a new graphical representation of the members of the Z-Octahedron family based on octagonal cells has been proposed. This new type of elementary cell has eight nodes and two struts, twice the number of nodes and struts than those found in rhombic and Z-shaped cells. The Z-triple-expanded octahedron has been obtained from the topology of the Z-Octahedron family considering the new octagonal connection graphs. This stable tensegrity structure is composed of 48 nodes, 24 struts, and 72 cables. The Z-triple-expanded octahedron contains both the Z-double-expanded octahedron and the Z-expanded octahedron as folded forms, which is a necessary condition for tensegrity families belonging to the same family. It has been proved that the new octagonal graphical representation of the Z-Octahedron family can be a good source of new tensegrity forms.

New tensegrity structures derived from the Z-Octahedron family have been defined. The connections between elements of the new octagonal cells have been modified leading to other types of octagonal cells (type 2 and type 3 octagonal cells). Super-stable tensegrity forms have been obtained analytically. In addition, several element groupings have been considered in order to obtain different equilibrium configurations of these new tensegrity structures. The introduction of additional cables in the elementary octagonal cell clearly results in an improvement of the stability of the resultant tensegrity and in a reduction of the force:length ratio in the cables in the equilibrium configuration.

Appendix A

A.1 Analytical form-finding of tensegrity structures (Fernández-Ruiz et al., 2019; Hernández-Montes et al., 2018)

An in-depth explanation of the analytical form-finding method of tensegrity structures employed in this work can be seen in (Fernández-Ruiz et al., 2019; Hernández-Montes et al., 2018). In this appendix, a summary of this method is presented.

The FDM (Linkwitz and Schek, 1971; Schek, 1974) is one of the most commonly used form-finding methods for general pin-jointed networks. The highly non-linear equilibrium equations are linearized by introducing the concept of force density or force:length ratio. The force:length ratio, q, is defined as the ratio between the axial force and the length of each member of the tensegrity. The equilibrium equations of a general

tensegrity composed of n nodes and m members (cables and struts) can be formulated as (Tran and Lee, 2010; Zhang and Ohsaki, 2015):

$$\begin{aligned} \mathbf{D}\,\mathbf{x} &= 0 \\ \mathbf{D}\,\mathbf{y} &= 0 \\ \mathbf{D}\,\mathbf{z} &= 0 \end{aligned} \tag{A.1}$$

In Eq. (A.1) $\mathbf{D} = \mathbf{C}^{\mathrm{T}}\mathbf{Q}\mathbf{C}$ ($\in \Re^{n\times n}$) is the force density matrix, and $\mathbf{x}$, $\mathbf{y}$, $\mathbf{z}$ ($\in \Re^{n}$) are the nodal coordinate vectors. The symbol $[]^{\mathrm{T}}$ represents the transpose operation of a matrix or vector. The inputs of the form-finding problem are connectivity matrix $\mathbf{C}$ and the force:length ratio, q, of each member of the tensegrity. Connectivity matrix $\mathbf{C}$ ($\in \Re^{m\times n}$) defines the connectivity between the nodes of the tensegrity. This matrix is constructed as follows: if a general member of j connects nodes i and k (with $i < k$), the ith and kth elements of the jth row of $\mathbf{C}$ are set to 1 and -1, respectively. Plane connection graphs are used to define matrix $\mathbf{C}$. On the other hand, vector $\mathbf{q} = (q_1, q_2, ..., q_m)$ ($\in \Re^{m}$) contains the force:length ratio of each member of the tensegrity ($\mathbf{Q}$ is the diagonal square matrix of vector $\mathbf{q}$).

In order to guarantee that a tensegrity does not lie in a space which has lower dimensions than the specific dimension d, matrix $\mathbf{D}$ should have rank deficiency of at least $d + 1$ (non-degeneracy condition (Hernández-Montes et al., 2018; Zhang and Ohsaki, 2006)). This non-degeneracy condition is achieved by making sure that the characteristic polynomial of $\mathbf{D}$ (see Eq. (A.2)) has at least $d + 1$ zero roots. Consequently, and in order to obtain a three-dimensional tensegrity ($d = 3$), coefficients a_3, a_2, a_1 and a_0 of the characteristic polynomial must be zero. Coefficient a_0 is always zero because matrix $\mathbf{D}$ is singular. Coefficients a_3, a_2 and a_1 are expressed in terms of the force:length ratios of the members of the tensegrity (q_1, q_2, …, q_m). The system of equations shown in Eq. (A.3) is analytically solved in order to obtain the force:length ratios of the members of the tensegrity that lead to a rank deficiency of matrix $\mathbf{D}$ of at least $d + 1$.

$$p(\lambda)=\lambda^{n}+a_{n-1}\lambda^{n-1}+\ldots+a_1\lambda+a_0 \tag{A.2}$$

$$\begin{aligned} a_3(q_1,\ldots,q_{\mathrm{m}}) &= 0 \\ a_2(q_1,\ldots,q_{\mathrm{m}}) &= 0 \\ a_1(q_1,\ldots,q_{\mathrm{m}}) &= 0 \end{aligned} \tag{A.3}$$

A.2 Stability, prestress-stability and super-stability of tensegrity structures

A tensegrity is stable if its corresponding tangent stiffness matrix $\mathbf{K} = \mathbf{K}_{\mathbf{GEOM}} + \mathbf{K}_{\mathbf{ELAST}}$ is a positive semi-definite matrix (Fernández-Ruiz et al., 2019; Zhang and Ohsaki, 2015,

2007). Matrix $\mathbf{K}_{\mathbf{ELAST}}$ is the elastic stiffness matrix and $\mathbf{K}_{\mathbf{GEOM}}$ is the geometric stiffness matrix. The stability of tensegrity structures, together with the definition of matrices $\mathbf{K}_{\mathbf{GEOM}}$ and $\mathbf{K}_{\mathbf{ELAST}}$, has been discussed in detail in (Fernández-Ruiz et al., 2019; Zhang and Ohsaki, 2015, 2007). In order to study the stability of a tensegrity, the material properties, A, (cross-sectional area) and, E, (Young's modulus) of its members must be known. In all the stability studies in this work, it is assumed that the maximum prestress is 1% of EA (Zhang and Ohsaki, 2015).

In preliminary studies, it could be useful to know whether a tensegrity with a specific pre-stressed state is stable or not, without considering any specific materials. A tensegrity is said to be prestress-stable if it is stable in the state of self-equilibrium in the directions of infinitesimal mechanisms (Zhang and Ohsaki, 2015). In this prestress-stability criterion, it is assumed that the member stiffness of the tensegrity is high enough.

Super-stability is a much higher stability criterion than previous ones. It has been stated that a tensegrity is super-stable if it is always stable, regardless of material properties and prestress levels (Connelly, 1998; Zhang and Ohsaki, 2015, 2007). The super-stability conditions of tensegrity structures are as follows (Connelly, 1998; Zhang and Ohsaki, 2015, 2007):

1. The rank deficiency of the force density matrix **D** is exactly $d + 1$.
2. The force density matrix **D** is positive semi-definite.
3. The rank of the matrix **G** is $(d^2 + d)/2$.

An in-depth explanation on the geometry matrix **G** can be seen in(Zhang and Ohsaki, 2015).

Data availability statement

The corresponding author will provide the script of the examples developed in this work on request.

References

Amendola, A., Krushynska, A., Daraio, C., Pugno, N.M., Fraternali, F., 2018. Tuning frequency band gaps of tensegrity mass-spring chains with local and global prestress. Int. J. Solids Struct. 155, 47–56. https://doi.org/10.1016/j.ijsolstr.2018.07.002

Bauer, J., Kraus, J.A., Crook, C., Rimoli, J.J., Valdevit, L., 2021. Tensegrity Metamaterials: Toward Failure-Resistant Engineering Systems through

481 Delocalized Deformation. Adv. Mater. 33, 1–9.
482 https://doi.org/10.1002/adma.202005647
483 Bel Hadj Ali, N., Rhode-Barbarigos, L., Pascual Albi, A.A., Smith, I.F.C., 2010. Design
484 optimization and dynamic analysis of a tensegrity-based footbridge. Eng. Struct.
485 32, 3650–3659. https://doi.org/10.1016/j.engstruct.2010.08.009
486 Boni, C., Royer-Carfagni, G., 2021. A new flexural-tensegrity bow. Mech. Mach.
487 Theory 164, 104398. https://doi.org/10.1016/j.mechmachtheory.2021.104398
488 Chen, M., Goyal, R., Majji, M., Skelton, R.E., 2020. Design and analysis of a growable
489 artificial gravity space habitat. Aerosp. Sci. Technol. 106, 106147.
490 https://doi.org/10.1016/j.ast.2020.106147
491 Connelly, R., 1998. Tensegrity structures. Why are they stable?, in: Thorpe, M.F.,
492 Duxbury, P.M. (Eds.), Rigidity Theory and Applications. Kluwer Academic /
493 Plenum Publishers, pp. 47–54.
494 Fernández-Ruiz, M.A., Hernández-Montes, E., Carbonell-Márquez, J.F., Gil-Martín,
495 L.M., 2019. Octahedron family: The double-expanded octahedron tensegrity. Int. J.
496 Solids Struct. 165, 1–13. https://doi.org/10.1016/j.ijsolstr.2019.01.017
497 Fernández-Ruiz, M.A., Hernández-Montes, E., Gil-Martín, L.M., 2022. Topological
498 design of the octahedron tensegrity family. Eng. Struct. 259, 114211.
499 https://doi.org/10.1016/j.engstruct.2022.114211
500 Fernández-Ruiz, M.A., Hernández-Montes, E., Gil-Martín, L.M., 2021. The Octahedron
501 family as a source of tensegrity families: The X-Octahedron family. Int. J. Solids
502 Struct. 208–209, 1–12. https://doi.org/10.1016/j.ijsolstr.2020.10.019
503 Fernández-Ruiz, M.A., Hernández-Montes, E., Gil-Martín, L.M., 2020. The Z-
504 octahedron family: A new tensegrity family. Eng. Struct. 222, 111151.
505 https://doi.org/10.1016/j.engstruct.2020.111151
506 Feron, J., Boucher, L., Denoël, V., Latteur, P., 2019. Optimization of Footbridges
507 Composed of Prismatic Tensegrity Modules. J. Bridg. Eng. 24.
508 https://doi.org/10.1061/(ASCE)BE.1943-5592.0001438
509 Fraldi, M., Cutolo, A., Carotenuto, A.R., Palumbo, S., Pugno, N., 2021. A lesson from
510 earthquake engineering for selectively damaging cancer cell structures. J. Mech.
511 Behav. Biomed. Mater. 119, 104533.
512 https://doi.org/10.1016/j.jmbbm.2021.104533
513 Fraternali, F., Carpentieri, G., Amendola, A., Skelton, R.E., Nesterenko, V.F., 2014.
514 Multiscale tunability of solitary wave dynamics in tensegrity metamaterials. Appl.

515 Phys. Lett. 105. https://doi.org/10.1063/1.4902071
516 Fraternali, F., Santos, F., 2019. Mechanical modeling of superelastic tensegrity braces
517 for earthquake-proof structures. Extrem. Mech. Lett. 33, 100578.
518 https://doi.org/10.1016/j.eml.2019.100578
519 Gómez-Jáuregui, V., 2010. Tensegrity structures and their application to architecture.
520 PubliCan, Ediciones de la Universidad de Cantabria.
521 Graells Rovira, A., Mirats Tur, J.M., 2009. Control and simulation of a tensegrity-based
522 mobile robot. Rob. Auton. Syst. 57, 526–535.
523 https://doi.org/10.1016/j.robot.2008.10.010
524 Hernández-Montes, E., Fernández-Ruiz, M.A., Gil-Martín, L.M., Merino, L., Jara, P.,
525 2018. Full and folded forms: a compact review of the formulation of tensegrity
526 structures. Math. Mech. Solids 23, 944–949.
527 https://doi.org/10.1177/1081286517697372
528 Kan, Z., Peng, H., Chen, B., Xie, X., Sun, L., 2019. Investigation of strut collision in
529 tensegrity statics and dynamics. Int. J. Solids Struct. 167, 202–219.
530 https://doi.org/10.1016/j.ijsolstr.2019.03.012
531 Lee, H., Jang, Y., Choe, J.K., Lee, S., Song, H., Lee, J.P., Lone, N., Kim, J., 2020. 3D-
532 printed programmable tensegrity for soft robotics. Sci. Robot. 5, 1–12.
533 https://doi.org/10.1126/SCIROBOTICS.AAY9024
534 Li, Y., Feng, X.Q., Cao, Y.P., Gao, H., 2010. Constructing tensegrity structures from
535 one-bar elementary cells. Proc. R. Soc. A Math. Phys. Eng. Sci. 466, 45–61.
536 https://doi.org/10.1098/rspa.2009.0260
537 Linkwitz, K., Schek, H.J., 1971. Einige Bemerkungen zur Berechnung von
538 vorgespannten Seilnetzkonstruktionen. Ingenieur-Archiv. 40, 145–158.
539 https://doi.org/10.1007/BF00532146
540 Liu, Y., Bi, Q., Yue, X., Wu, J., Yang, B., Li, Y., 2022. A review on tensegrity
541 structures-based robots. Mech. Mach. Theory 168, 104571.
542 https://doi.org/https://doi.org/10.1016/j.mechmachtheory.2021.104571
543 Ma, Y., Zhang, Q., Dobah, Y., Scarpa, F., Fraternali, F., Skelton, R.E., Zhang, D.,
544 Hong, J., 2018. Meta-tensegrity: Design of a tensegrity prism with metal rubber.
545 Compos. Struct. 206, 644–657. https://doi.org/10.1016/j.compstruct.2018.08.067
546 Murakami, H., Nishimura, Y., 2001. Static and dynamic characterization of regular
547 truncated icosahedral and dodecahedral tensegrity modules. Int. J. Solids Struct.
548 38, 9359–9381. https://doi.org/10.1016/S0020-7683(01)00030-0

549 Pugh, A., 1976. An introduction to tensegrity. University of California Press.
550 Rhode-Barbarigos, L., Hadj Ali, N.B., Motro, R., Smith, I.F.C., 2010. Designing
551 tensegrity modules for pedestrian bridges. Eng. Struct. 32, 1158–1167.
552 https://doi.org/10.1016/j.engstruct.2009.12.042
553 Schek, H.J., 1974. The force density method for form-finding and computation of
554 general networks. Comput. Methods Appl. Mech. Eng. 3, 115–134.
555 https://doi.org/10.1016/0045-7825(74)90045-0
556 Singh, N., Amendola, A., Santos, F., Benzoni, G., Fraternali, F., 2020. Mechanical
557 response of tensegrity dissipative devices incorporating shape memory alloys. IOP
558 Conf. Ser. Mater. Sci. Eng. 999. https://doi.org/10.1088/1757-899X/999/1/012001
559 Suma, A., Coronel, L., Bussi, G., Micheletti, C., 2020. Directional translocation
560 resistance of Zika xrRNA. Nat. Commun. 11, 1–9. https://doi.org/10.1038/s41467-
561 020-17508-7
562 Tibert, A.G., Pellegrino, S., 2002. Deployable Tensegrity Reflectors for Small
563 Satellites. J. Spacecr. Rockets 39, 701–709. https://doi.org/10.2514/2.3867
564 Tran, H.C., Lee, J., 2010. Advanced form-finding of tensegrity structures. Comput.
565 Struct. 88, 237–246. https://doi.org/10.1016/j.compstruc.2009.10.006
566 Veuve, N., Dalil Safaei, S., Smith, I.F.C., 2016. Active control for mid-span connection
567 of a deployable tensegrity footbridge. Eng. Struct. 112, 245–255.
568 https://doi.org/10.1016/j.engstruct.2016.01.011
569 Xu, X., Wang, Y., Luo, Y., 2016. General Approach for Topology-Finding of
570 Tensegrity Structures. J. Struct. Eng. 142, 04016061.
571 https://doi.org/10.1061/(asce)st.1943-541x.0001532
572 Xu, X., Wang, Y., Luo, Y., Hu, D., 2018. Topology Optimization of Tensegrity
573 Structures Considering Buckling Constraints. J. Struct. Eng. 144, 04018173.
574 https://doi.org/10.1061/(asce)st.1943-541x.0002156
575 Yin, X., Gao, Z.Y., Zhang, S., Zhang, L.Y., Xu, G.K., 2020. Truncated regular
576 octahedral tensegrity-based mechanical metamaterial with tunable and
577 programmable Poisson's ratio. Int. J. Mech. Sci. 167, 105285.
578 https://doi.org/10.1016/j.ijmecsci.2019.105285
579 Zhang, J.Y., Ohsaki, M., 2015. Tensegrity Structures. Form, Stability, and Symmetry.
580 Springer.
581 Zhang, J.Y., Ohsaki, M., 2007. Stability conditions for tensegrity structures. Int. J.
582 Solids Struct. 44, 3875–3886. https://doi.org/10.1016/j.ijsolstr.2006.10.027

583 Zhang, J.Y., Ohsaki, M., 2006. Adaptive force density method for form-finding
584 problem of tensegrity structures. Int. J. Solids Struct. 43, 5658–5673.
585 https://doi.org/10.1016/j.ijsolstr.2005.10.011
586 Zhang, J.Y., Ohsaki, M., Tsuura, F., 2019. Self-equilibrium and super-stability of
587 truncated regular hexahedral and octahedral tensegrity structures. Int. J. Solids
588 Struct. 161, 182–192. https://doi.org/10.1016/j.ijsolstr.2018.11.017
589 Zhang, L.Y., Jiang, J.H., Wei, K., Yin, X., Xu, G.K., Zhang, J., 2021. Self-equilibrium
590 and super-stability of rhombic truncated regular tetrahedral and cubic tensegrities
591 using symmetry-adapted force-density matrix method. Int. J. Solids Struct. 233,
592 111215. https://doi.org/10.1016/j.ijsolstr.2021.111215
593 Zhang, L.Y., Li, Y., Cao, Y.P., Feng, X.Q., 2013. A unified solution for self-
594 equilibrium and super-stability of rhombic truncated regular polyhedral
595 tensegrities. Int. J. Solids Struct. 50, 234–245.
596 https://doi.org/10.1016/j.ijsolstr.2012.09.024